Highly oriented photosynthetic reaction centers generate a proton gradient in synthetic protocells

Emiliano Altamura[a], Francesco Milano[b], Roberto R. Tangorra[a], Massimo Trotta[b], Omar Hassan Omar[c], Pasquale Stano[d,1], and Fabio Mavelli[a,2]

[a]Chemistry Department, University of Bari Aldo Moro, I-70126 Bari, Italy; [b]Institute for Physical and Chemical Processes, Italian National Research Council, I-70126 Bari, Italy; [c]Institute of Chemistry of Organometallic Compounds, Italian National Research Council, I-70126 Bari, Italy; and [d]Science Department, Roma Tre University, I-00146 Rome, Italy

Edited by Steven G. Boxer, Stanford University, Stanford, CA, and approved February 9, 2017 (received for review October 23, 2016)

Photosynthesis is responsible for the photochemical conversion of light into the chemical energy that fuels the planet Earth. The photochemical core of this process in all photosynthetic organisms is a transmembrane protein called the reaction center. In purple photosynthetic bacteria a simple version of this photoenzyme catalyzes the reduction of a quinone molecule, accompanied by the uptake of two protons from the cytoplasm. This results in the establishment of a proton concentration gradient across the lipid membrane, which can be ultimately harnessed to synthesize ATP. Herein we show that synthetic protocells, based on giant lipid vesicles embedding an oriented population of reaction centers, are capable of generating a photoinduced proton gradient across the membrane. Under continuous illumination, the protocells generate a gradient of 0.061 pH units per min, equivalent to a proton motive force of 3.6 mV·min^{-1}. Remarkably, the facile reconstitution of the photosynthetic reaction center in the artificial lipid membrane, obtained by the droplet transfer method, paves the way for the construction of novel and more functional protocells for synthetic biology.

photosynthetic reaction center | giant lipid vesicles | artificial cells | light transduction | proton gradient

The synthesis of living cells from scratch is one of the most ambitious goals in biology and chemistry (1–6). Initiated in the origin-of-life community (7–10), research on supramolecular assemblies modeling primitive cells has rapidly increased in the past few years. More recently the rapid expansion of synthetic biology (11) has given additional conceptual stimuli and technical tools to this field, especially by the so-called bottom-up approach (12). Despite the recent progress, which is mainly focused on the reconstitution of essential biochemical functions inside confined environments (13) such as phospholipid (4, 5, 14–19) and fatty acid vesicles (8, 20, 21), water-in-oil (w/o) droplets (22), and coacervates (23), the primary generation of chemical energy by molecular machineries remains a missing key function.

In this paper we try to fill this gap by constructing protocells capable of transducing light into chemical energy in the form of a pH gradient. To this aim, the photosynthetic reaction center (RC) extracted from *Rhodobacter sphaeroides* has been reconstituted in giant lipid vesicles. RC is a membrane-spanning protein located in biological membranes surrounded by other chlorophyll- based proteins (see *SI Appendix*, section S3a for a detailed description) (24, 25) and it is the core of the photosynthetic apparatus of plants, algae, and photosynthetic bacteria. However, if extracted from living systems and reconstituted in suitable lipid compartments it can also work in the absence of its ancillary proteins. RC is composed of two highly hydrophobic subunits, L and M, and the mostly hydrophilic H subunit (26). These subunits cooperate, by a mechanism based on photon absorption (27), to catalyze the reduction of quinone species, removing protons from the cytoplasm (*SI Appendix*, Figs. S1 and S2 *A* and *B*). The RC photocycle (illustrated in *SI Appendix*, Fig. S2*C*) starts when RC absorbs a photon and generates an electron-hole couple in the presence of an electron donor (reduced cytochrome c_2) and an electron acceptor (ubiquinone). While reduced cytochromes c_2 transfer electrons to RC from the external pool, protons are taken up from the cytoplasm by ubiquinone, giving ubiquinol, thus establishing a pH gradient across the intracytoplasmic membrane. The proton gradient is used by the cell to fuel ATP synthesis (28) and ultimately the whole metabolism of the organism (29).

Previous work (30–40) has shown that RC can be reconstituted with the detergent depletion method (41), generally with random orientation in submicrometer liposomes (31, 34, 35, 37–40). However, partial (60%) (33) and high physiological orientation (90%) (30) have also been reported, and it has been shown that experimental conditions play a decisive role in determining RC orientation (32, 36, 42). RC reconstitution has been reported in random orientation in planar lipid bilayers (43–46) as well, even if high orientation can be also achieved in such systems (42). We have already reported the generation of a transmembrane proton gradient in RC-containing conventional liposomes (40). Herein we present a single-step procedure for reconstituting RC in giant lipid vesicles with high physiological orientation, showing that the resulting RC@GUVs (GUVs with RC reconstituted in the lipid membrane) are able to convert light into a transmembrane pH gradient.

Results

Reconstitution of RC in Giant Unilamellar Vesicle Membrane by Means of the Droplet Transfer Method. Giant unilamellar vesicles (GUVs) (47) were prepared using the droplet transfer method (48) (Fig. 1)

Significance

The photosynthetic reaction center (RC), an integral membrane protein at the core of bioenergetics of all autotrophic organisms, has been reconstituted in the membrane of giant unilamellar vesicles (RC@GUV) by retaining the physiological orientation at a very high percentage (90 ± 1%). Owing to this uniform orientation, it has been possible to demonstrate that, under red-light illumination, photosynthetic RCs operate as nanoscopic machines that convert light energy into chemical energy, in the form of a proton gradient across the vesicle membrane. This result is of great relevance in the field of synthetic cell construction, proving that such systems can easily transduce light energy into chemical energy eventually exploitable for the synthesis of ATP.

Author contributions: E.A., F. Milano, and F. Mavelli designed research; E.A. performed research; O.H.O. synthesized the AE-NHS fluorephore; F. Milano, R.R.T., M.T., and P.S. contributed new reagents/analytic tools; E.A., M.T., P.S., and F. Mavelli analyzed data; E.A., M.T., P.S., and F. Mavelli wrote the paper; and F. Mavelli carried out numerical analysis and stochastic simulations.

The authors declare no conflict of interest.

This article is a PNAS Direct Submission.

See Commentary on page 3790.

[1]Present Address: Department of Biological and Environmental Sciences and Technologies, University of Salento, I-73100 Lecce, Italy.

[2]To whom correspondence should be addressed. Email: fabio.mavelli@uniba.it.

This article contains supporting information online at www.pnas.org/lookup/suppl/doi:10.1073/pnas.1617593114/-/DCSupplemental.

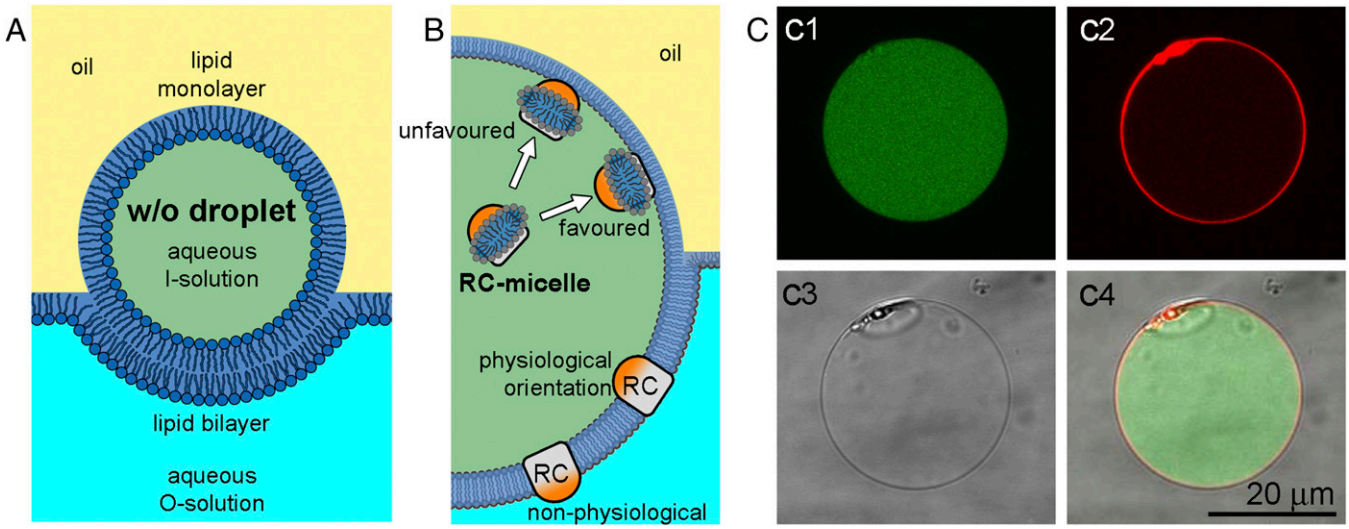

Fig. 1. Preparation of GUVs by the droplet transfer method (48). (*A*) Water in oil (w/o) droplets, prepared by the emulsification of an aqueous solution (I-solution) in a lipid-rich oil phase, are transferred to an aqueous solution (O- solution) by centrifugation. (*B*) For preparing RC@GUVs, a detergent-stabilized RC solution (RC-micelles) is emulsified in oil, giving the w/o droplets. Owing to asymmetric RC-micelle structure a preferential "physiological" RC orientation is expected, namely, with the H subunit (in orange) facing toward the aqueous core of the droplets (the cytoplasm-like GUV lumen), and the photoactive dimer (*SI Appendix*, Fig. S2 *A* and *B*) facing the GUV exteriors (in white). (*C*) RC@GUVs (POPC:POPG, 9:1) as imaged by confocal microscopy. Red-fluorescent AE-RC was reconstituted in calcein-containing GUVs. (*C1*) Green fluorescence channel (calcein). (*C2*) Red fluorescence channel (AE-RC). (*C3*) Bright field. (*C4*) Overlay of the *C1*, *C2*, and *C3* channels.

because we envisaged that this method could be suitable for reconstituting transmembrane proteins with a high degree of physiological orientation. Purified RC from *R. sphaeroides* was first obtained by a well-established procedure requiring the detergent lauryldimethylamine *N*-oxide (LDAO) to extract the protein from the photosynthetic membrane and to solubilize it in aqueous solutions (49). A homogeneous micellar solution was obtained with fully photoactive RCs surrounded by a toroid of LDAO molecules that shield the LM core from the aqueous environment (50). To prepare RC@GUVs, the RC micelle solution was emulsified in mineral oil containing a mixture of phosphatidylcholine and phosphatidylglycerol (POPC:POPG, 9:1). This emulsion was then layered on the aqueous solution, generating a biphasic system, and RC@GUVs were obtained after centrifugation (Fig. 1*C*).

Considering the RC reconstruction mechanism in vesicle membrane, it is reasonable to assume that micelles when dispersed in w/o will deliver their protein cargo at the droplet w/o interface, mainly driven by hydrophobic interactions. Moreover, because RCs present asymmetric distribution of hydrophilic and hydrophobic regions, protein-containing micelles will have a preferential orientation while approaching, and interacting with, the lipid monolayer of the w/o droplet, because the large hydrophilic H subunit prefers the aqueous phase (*SI Appendix*, Fig. S2 *A* and *B*). It is expected that the chemical vectoriality of both RC-micelles and lipid monolayer will favor only one of the possible protein orientations in the w/o droplets before and during their transfer to the aqueous phase, so that a population of highly oriented RCs in the GUVs membrane should be obtained.

RC@GUVs prepared in such a way have an average diameter of 20 ± 10 µm (statistical analysis performed on a population of 150 GUVs; *SI Appendix*, Fig. S3) and are morphologically stable for at least 2 d when stored in the dark at room temperature. Quantitative image analysis shows calcein does not leak out from GUVs after 2 d from the preparation (*SI Appendix*, Fig. S4), proving also that traces of detergent, present as a consequence of the RC encapsulation, do not significantly affect the membrane stability.

The concentration of lipids and photoactive RCs, collected in a 100-µL volume of the thus-prepared GUVs suspension, was determined spectroscopically (*SI Appendix*, section S2g), resulting 440 µM and 0.2 µM, respectively, and hence a protein/lipid molar ratio of 1/2,200 was reached. RC@GUVs are characterized by a quite high RC density (~1,200 RC molecules per μm^2), corresponding to roughly one-third of the RC average density in the intracytoplasmic membranes of photosynthetic bacteria (51, 52). The collected GUVs were washed twice before further use, to remove any external fragments of RCs.

Fluorescently labeled RCs were used to monitor the spatial distribution of the protein in GUVs. As a fluorophore we selected a suitable fluorescent dye belonging to the aryleneethynylenes class, because these molecules emit (53) light efficiently and can be easily functionalized to be covalently conjugated to biomolecules (*SI Appendix*, section S2a). In this work, we used the 7-AE fluorophore (AE) (*SI Appendix*, Fig. S6) (54), which absorbs light at 445 nm and emits it in the red region at 602 nm (*SI Appendix*, Fig. S7). The AE is covalently linked through an amide bond to the protein lysine residues by exploiting the succinimidyl *N*-hydroxysuccinimidyl ester derivative AE-NHS as an activated compound toward the reaction with amine groups in the lysines (*SI Appendix*, Fig. S8) (54). The AE-RC conjugate can be easily visualized by confocal microscopy, allowing its localization in AE-RC@GUVs. Fig. 2*C* shows images obtained by confocal laser scanning microscopy where vesicles display a uniform red fluorescent ring overlapping with the vesicle membrane, demonstrating a homogeneous incorporation of RC in the lipid bilayer of all GUVs.

RC Is Active and Highly Oriented. The photoactivity of reconstituted RC can be assessed by inducing the formation of an electron-hole couple by a short light flash and monitoring the time of the charge recombination reaction by following the absorbance at 865 nm (the detailed mechanism is reported in *SI Appendix*, section S3b). Fig. 2 shows the time decay of the charge-separated state induced by light flash: blue dots are the recovery of the dimer signal from the excited state after a saturating flash in RCs reconstituted in giant vesicles. From the initial absorbance, $\Delta A_{865}(0) = 2.21 \pm 0.03$ milliabsorbance (mAU), the actual RC amount in the RC@GUVs preparation can be determined, which corresponds to ~10% of the protein initially loaded in the w/o droplets. The biexponential fitting of the recorded trace (blue line) reveals that the fast charge-recombination from $D^+Q_A^{-\bullet}$ (A_f) accounts for about 71% of the overall signal, whereas the slow recombination from $D^+Q_AQ_B^{-\bullet}$ (A_s) contributes in a minor way (29%), showing that under these experimental conditions the Q_B-site

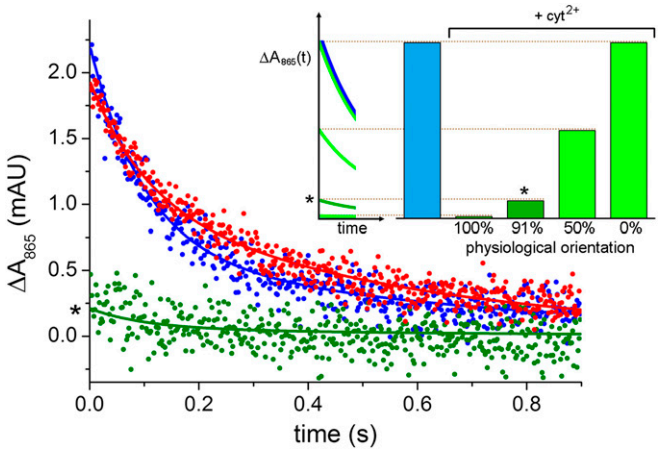

Fig. 2. Charge recombination of RCs reconstituted in giant vesicles after a saturating light flash. The points represent the experimental data, and the lines are the biexponential best fit curves. Data refer to charge recombination in the absence (blue points) and in the presence (dark green points) of excess of reducing agent (cyt^{2+}). In a control experiment (red points), a full recovery of RC photoactivity is measured after the addition of an electron acceptor, the dQ, and the exhaustion of cyt^{2+}. Note that values in the *y* axis represent the absolute values of ΔA_{865}. (*Inset*) Theoretical charge recombination curves in the absence (blue) and in the presence (green) of cyt^{2+}, corresponding to different RC orientation (100, 50, and 0% of physiological orientation). The histogram represents the initial amplitude of the curves $\Delta A_{865}(0)$. The green bar marked with the asterisk refers to the experimental trace reported in the main plot.

is only occupied partially (Table 1, first row). The orientation of the RC population in GUV membrane can be assessed by using the water-soluble cytochrome c_2 (30), the physiological electron donor to the photooxidized dimer. In fact, both the reduced (cyt^{2+}) and the oxidized (cyt^{3+}) forms of the cytochrome are unable to cross the membrane. Therefore, the reduced cyt^{2+} added in excess externally to preformed RC@GUVs reacts only with the oxidized dimers exposed to the outer solution. The electron donation from the reduced cytochrome to the oxidized dimer, $D^+ + cyt^{2+} \rightarrow D + cyt^{3+}$, occurs very fast on the microsecond time scale, preventing the charge recombination reaction. The dimers reduced by the cyt^{2+} will not contribute to the absorbance recorded at 865 nm. On average, if the RCs reconstituted in the GUVs dispose across the lipid bilayer in random orientation, only half of the dimers face toward the bulk solution. Under this condition, a saturating flash of light will generate the full population of D^+, but the signal will appear halved because the dimers oriented toward the bulk are rereduced on a very fast time scale by cyt^{2+}. The other extreme possibilities, that is, fully oriented RCs with the dimer facing the GUVs core, or fully oriented with the dimer facing the external aqueous solution, will give the full signal $\Delta A_{865}(0)$ in the presence of cyt^{2+} or the complete absence of signal, respectively (Fig. 2, *Inset*). The actual ratio of the D^+ absorbance change in the presence $[\Delta A_{865}(0)_{cyt}]$ and in the absence $[\Delta A_{865}(0)]$ of cyt^{2+} gives the fraction of RCs oriented in the bilayer with the dimer exposed to the outer solution. Hence, fully oriented RCs will have the ratio $\Delta A_{865}(0)_{cyt}/\Delta A_{865}(0)$ value equal to 0 when all RCs are oriented with the dimer outward. The ratio assumes a value of 1 when all RCs are oriented with the dimer facing the GUV water core. All other intermediate possibilities will have a ratio value ranging from 0 to 1.

Fig. 2 (green points) shows the recovery of D in RC@GUVs in the presence of externally added cyt^{2+}. A small signal $\Delta A_{865}(0)_{cyt}$ 0.21 ± 0.01 mAU is recorded, accounting for 9.5 ± 0.6% of the $\Delta A_{865}(0)$ value recorded in the absence of cyt^{2+} (Table 1, second row). This clearly indicates that the vast majority of photoactive proteins in RC@GUVs prepared by the droplet transfer method, 90 ± 1%, are uniformly oriented and expose the dimer to the outer aqueous phase. Notably, this result also demonstrates that the large majority of vesicles prepared by the droplet transfer method are unilamellar, as reported elsewhere (55). In fact, if RC were embedded in any internal lipid structure, as in the internal membranes of multilamellar vesicles, it would not react with cyt^{2+} and therefore it would count as oppositely oriented.

As a further experimental test to check RC functionality, a suitable amount of decylubiquinone (dQ) was then added to oxidize all cyt^{2+} molecules, as a result of the RC photocycle (*SI Appendix*, Fig. S2*C*). In fact, dQ is a ubiquinone analogous that binds to the RC Q_B-site and accepts electrons as well (56). When added to RC@GUVs suspension, it is expected that dQ will insert into the lipid membrane and diffuse and bind to RC Q_B-site. RC@GUVs were illuminated with repeated light pulses until the exhaustion of cyt^{2+}, which is converted to cyt^{3+}, whereas dQ is reduced to decylhydroubiquinone dQH_2. Thus, having removed all of the exogenous electron donors, the charge recombination signal reappeared. As shown in Fig. 2 (red points) and Table 1 (third row), the measured ΔA_0 value, in the presence of dQ (1.94 ± 0.03 mAU), is close to the original 2.21 ± 0.03 mAU value, demonstrating unequivocally the biochemical activity and the high orientation of RCs in GUVs. As expected, the slow pathway for charge recombination (k_s = 1.86 ± 0.06 s^{-1}) now becomes more relevant (55%), due to the presence of dQ in the Q_B-site.

RC Converts Light Energy into a pH Gradient Across the GUV Membrane. The spontaneously achieved high orientation of RCs in the bilayer of the GUVs having roughly 90% of the dimer facing the aqueous bulk and, consequently, ∼90% of the Q_B-site facing the vesicle lumen, can be exploited to efficiently build a light-driven pH gradient across the GUV membrane. Under continuous actinic illumination, and thanks to the electron-hole couple formation, the electrons will flow from the external donor (cyt^{2+}) to the acceptor (dQ in the Q_B-site) that will uptake protons from the vesicle aqueous core to form the quinol dQH_2. Ultimately, this compound accumulates in the bilayer. The net result of the photocycle is an intravesicle alkalinization that can be revealed using the pH-sensitive probe pyranine. Pyranine-containing RC@GUVs, prepared with low buffer capacity, were hence added with an excess of dQ, a small amount of cyt^{2+}, and an excess of ferrocyanide acting as secondary electron donor. Under continuous irradiation, the pathway shown in Fig. 3 is established. The net stoichiometry of the main process is the oxidation of two ferrocyanides to ferricyanide, and the reduction of dQ to dQH_2,

$$2Fe(CN)_6^{4-} + dQ + 2H^+ \xrightarrow{2h\nu} 2Fe(CN)_6^{3-} + dQH_2,$$

removing two protons per dQ molecule from the vesicle lumen.

Continuous red-light irradiation of pyranine-containing RC@GUVs (*SI Appendix*, Fig. S9) generated an increase of pyranine fluorescence over the whole vesicle population, shown in Fig. 4*A* for two different RC concentrations in the final suspension: 10 and 20 nM, respectively. As can be seen, by doubling the RC concentration in the preparation this amplifies the pH-increase rate by a factor of 2.11 ± 0.02.

Table 1. Kinetic analysis of charge recombination experiments

Sample	ΔA_0, mAU	A_f, %	A_s, %	k_s, s^{-1}
RC@GUVs	2.21 ± 0.03	71 ± 3	29 ± 3	1.52 ± 0.09
RC@GUVs + cyt^{2+}	0.21 ± 0.01	71 ± 13	29 ± 13	1.50 ± 0.10
RC@GUVs + cyt^{2+} + dQ	1.94 ± 0.03	45 ± 2	55 ± 2	1.86 ± 0.06

Biexponential decay fitting of experimental data reported in Fig. 2. Further details are given in *SI Appendix*, section S3b.

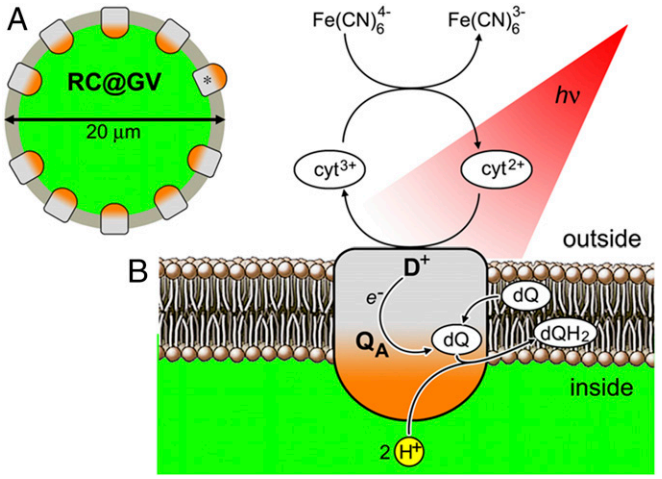

Fig. 3. Scheme of RC@GUVs function under red-light illumination. (*A*) RC is reconstituted in a highly oriented manner (90%) in the membrane of GUVs, whose average diameter is 20 μm. The asterisk marks a nonphysiologically oriented RC. (*B*) Detail of the photochemical mechanism generating the pH gradient. *hv*, light energy.

The incipient proton gradient across the membrane of individual RC@GUVs was visualized by directly illuminating the vesicles in a microscopy slide well and imaging them with confocal microscopy. Fig. 4*B* reports a series of fluorescence micrographs referring to pyranine-containing RC@GUVs at increasing irradiation time. Pyranine fluorescence increases over time as expected and the fluorescence intensity obtained by image analysis was converted to pH units via a calibration curve (*SI Appendix*, Fig. S10). The internal pH linearly increases in time, as shown in Fig. 4*C*, with a slope of 0.061 pH unit per min, equivalent to one pH unit in 16.4 min. The average rate of pH increase was converted in the rate of translocated proton per RC by a physicochemical model that takes into account the GUV size, the RC density, and chemical composition of the vesicle lumen. According to some simplifying assumptions (detailed in *SI Appendix*, sections S5 c and e) the observed pH increase corresponds to a calculated RC turnover rate of about 1.0 ± 0.1 protons per min per protein, equivalent to 2.5×10^6 protons per min per GUV. This value is our best estimate of RC function in GUVs in current experimental conditions and corresponds to about 10% of the maximal RC turnover rate calculated from the photon flux density delivered to the microscope well (*SI Appendix*, section S5e). Moreover, it contributes for a proton motive force of *ca.* 3.6 mV·min^{-1} (ΔpH min^{-1} × 59 mV). To test the robustness of the RC@GUV, the same sample was irradiated in a fluorimetric cuvette for 30 min immediately after the preparation and later on 24 h (stored in the dark at room temperature) by showing a comparable increase in the fluorescence of the encapsulated pyranine (*SI Appendix*, Fig. S11). These experiments show that GUVs retain the encapsulated pyranine and, at the same time, that the RC activity is largely (*ca.* 80%) maintained (*SI Appendix*, section S3c).

Moreover, based on the developed kinetic model (*SI Appendix*, section S5b), a statistical estimation of the pH change over time in the entire GUV population was obtained taking into account the vesicle polydispersity in size and in RC content. Because the GUV size distribution is experimentally known (*SI Appendix*, Fig. S13), by assuming a random distribution for the RC surface concentration it is possible to derive the bivariate density function $P_{Ves}(D, C_{RC})$ that estimates the probability $P_{Ves}(D, C_{RC})\, dD\, dC_{RC}$ to find a GUV with diameter in the $[D, D + dD[$ range and RC concentration in the $[C_{RC}, C_{RC} + dC_{RC}[$ interval (*SI Appendix*, Fig. S14). According to this model, the calculated displacements of the pH time course, weighted by the density probability $P_{Ves}(D, C_{RC})$ for the whole vesicle population, are reported as a green band (1–60 μm) in Fig. 4*D*. The shown large diversity in GUV performances depends much more on the vesicles size dispersion than on the random distribution of the RC proteins in the lipid membrane. In fact, the red band, which refers to vesicles with a restricted size range (15–30 μm), exhibits a more uniform behavior (Fig. 4*B* and *SI Appendix*, Fig. S16) that is much closer to those of the GUVs monitored experimentally. The comparison with the experimental data are good enough to validate the theoretical approach, although a statistical analysis on a larger vesicle population would be necessary. Because the number of RCs per GUV scales with the vesicle surface, whereas the variations of the proton concentration scales with the GUV volume, the model predicts small RC@GUVs generate a pH gradient faster than large ones (*SI Appendix*, Fig. S15). It is also possible to estimate theoretically the behavior of the smaller RC@GUVs with diameters in the <12.5-μm range that represent the 27% of the entire population and remove intravesicle protons from two to four times faster than the average (*SI Appendix*, Fig. S15), resulting in a theoretical pH increase rate up to 0.106 pH units per min. This suggests that RC@GUV with optimized size in the range between 10–15 μm would perform more efficiently and uniformly than those shown in this first report. Microfluidics fabrication could be used to produce almost completely monodispersed vesicle samples.

Conclusions

By using the droplet transfer method we have shown here the construction of an artificial cell model, based on bacterial RC, capable of transducing light into chemical energy. The reconstitution of RCs in the GUV membrane results in a uniform orientation ($90 \pm 1\%$) with the dimer of the photoenzyme facing the outer aqueous solution. This orientation reproduces the disposition of the proteins in the natural photosynthetic membrane, allowing the establishment of a light-induced pH change as in photosynthetic bacteria in this biomimetic system. Furthermore, these synthetic protocells show an RC surface density comparable to the in vivo intracytoplasmic membranes (52). The measured proton translocation rate, 1.0 ± 0.1 protons per min per RC, generates chemical energy in the form of a pH gradient that can be eventually converted in chemical work. However, more in-depth analyses are required to investigate how vesicle size, membrane lipid compositions, and trace amounts of residual detergent can affect the RC reconstitution, the RC@GUVs yield, the membrane permeability, and the RC photoactivity, paving the way for future optimization.

According to the presented methodology, other membrane proteins could be reconstituted in GUVs (57) (i.e., ATP-synthase, which would transduce the RC-generated proton gradient to ATP synthesis). A preliminary analysis suggests that the topological features of ATP-synthase would allow its reconstitution in the desired orientation in RC-containing lipid vesicles, so that ATP can be produced within the GUV lumen. This sharply contrasts with the usual reconstitution procedures of photosynthetic protein complexes (58–60) or artificial photosynthetic systems (61) where ATP is produced outside the vesicles. The presented study represents a step forward in the aim of assembling artificial cells capable of autonomously generating chemical energy.

Methods

Purification of RC. Photosynthetic RC was purified from the α-protobacterium *R. sphaeroides* (R-26 strain) according to a reported protocol (49), obtaining an aqueous solution of RC micelles stabilized by LDAO (0.03% wt/vol =1.3 mM) in 20 mM Tris·HCl (pH 8.0) and 1 mM EDTA. RC-AE conjugate was prepared in the same buffer but in the presence of Triton X-100 (0.03% wt/vol = 0.48 mM) as described in *SI Appendix*, section S2b.

Preparation of Giant Vesicles. RC reconstitution in GUVs was carried out by droplet transfer method (39), which consists of transforming micrometer-sized lipid-stabilized w/o droplets in GUVs. The method employs the following three solutions: (*i*) the organic phase, consisting of 0.5 mM POPC/POPG 9/1 mol/mol dissolved in mineral oil; (*ii*) the inner solution (I-solution), consisting of a freshly prepared RC-containing mixture (10 μM RC or AE-RC, 0.003% detergent, 5 mM

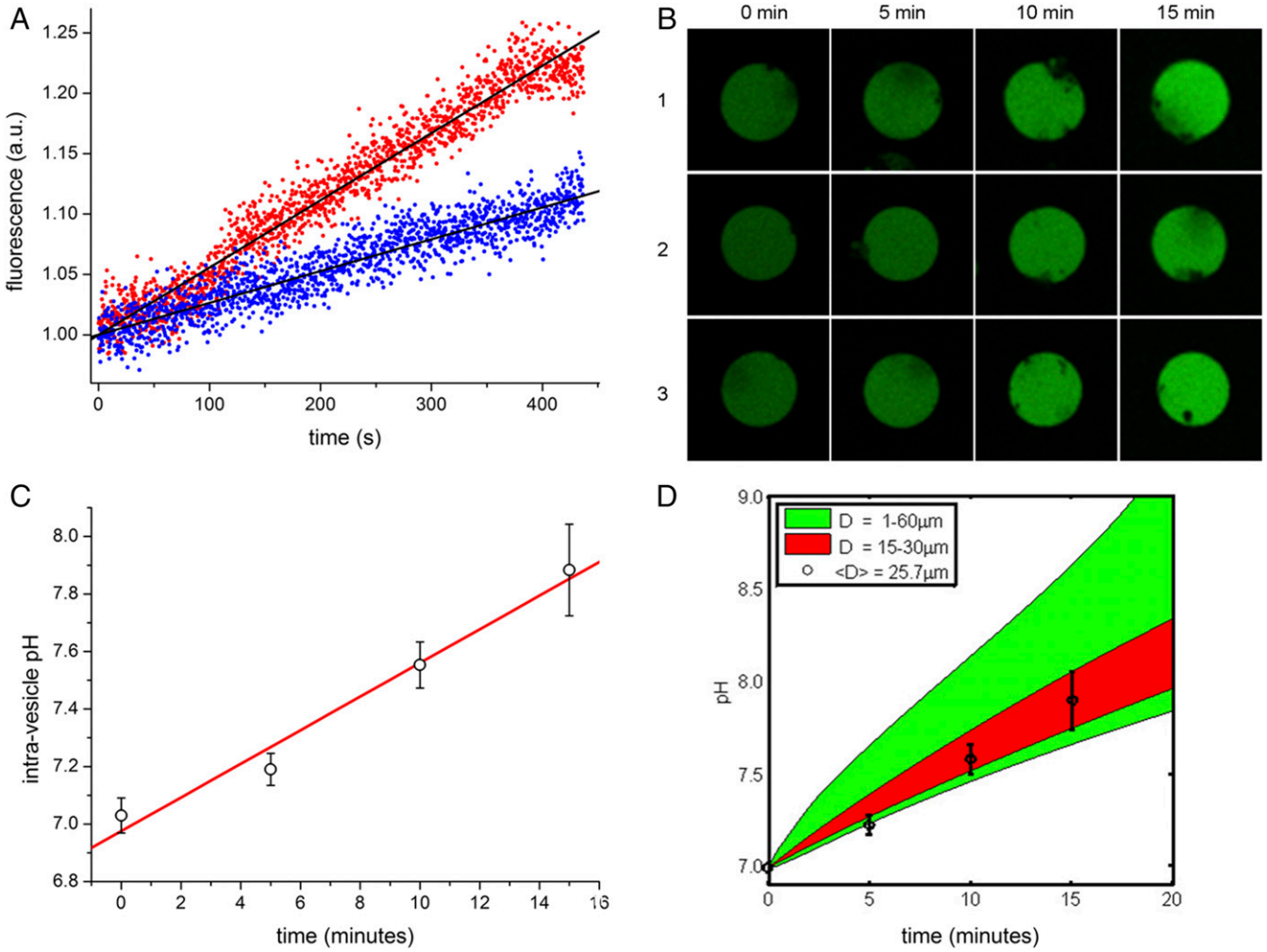

Fig. 4. Generation of a pH gradient by RC@GUVs. (*A*) Bulk fluorescence measurements of pyranine-containing RC@GUVs, which have been suspended in a fluorescence cuvette and illuminated from the top (*SI Appendix*, Fig. S9). Blue and red points refer to RC@GUVs with final RC concentration of 10 nM and 20 nM, respectively. Black lines represent the best-fit straight line, whose slopes are $(2.64 \pm 0.03) \times 10^{-4}$ a.u.·min^{-1} and $(5.57 \pm 0.03) \times 10^{-4}$ a.u.·min^{-1}, respectively, for the blue and red datasets. (*B*) Confocal images of three pyranine-containing RC@GUVs illuminated with red light. (*C*) Quantitative image analysis reveals the increase of intravesicle pH in time (fluorescence values converted by means of a calibration; *SI Appendix*, section S2h). The best-fit slope is 0.061 ± 0.004 pH units per min. (*D*) Comparison between the experimentally observed pH increase in the aqueous core of giant vesicles: circles with error bars (as in *C*) and the theoretical outcomes (colored bands). a.u., arbitrary units.

Tris·HCl buffer, pH 7.4 or 10 μM Tris·HCl buffer, pH ∼7.0, and 200 mM sucrose); and (*iii*) the outer solution (O-solution) consisting of a freshly prepared 5 mM Tris·HCl buffer, pH 7.4 or 10 μM Tris·HCl buffer, pH ∼7.0 and 200 mM glucose. GUVs are collected after 10 min of centrifugation at 2,500 × *g* at room temperature (more details are given in *SI Appendix*, section S2d) and washed twice before being used. Note that the overall LDAO:lipid molar ratio is 1:170.

Charge Recombination Experiments. The RC@GUVs sample was diluted 1:8 with O-solution and placed in a 1-cm squared quartz fluorescence cuvette. GUVs were irradiated by xenon lamp flashes (∼100 μs) placed orthogonal with respect to the measuring beam. The absorbance decay at 865 nm (ΔA_{865}), which mirrors the charge recombination in RC, was followed in time (for about 2 s). Data were collected onto a digital oscilloscope (Tektronics TDS-3200), and multiple traces ($n = 64$, delay time 2 s) were averaged to reach a sufficiently high signal-to-noise ratio. The concentration of the photoactive protein was estimated using $\Delta\varepsilon_{865} = 112{,}000$ M^{-1}·cm^{-1} (*SI Appendix*, ref. 4).

Orientation Assay. Reduced cytochrome c_2 (cyt^{2+}, 5 μM)—freshly prepared by reduction of cyt^{3+} with ascorbate and purified by gel filtration chromatography on Sephadex G-25—was added to RC@GUVs, and charge recombination was measured as indicated above. The fraction of oriented RC is obtained by comparing the initial amplitude of the charge recombination absorbance decay recorded in the presence $\Delta A_{865}(0)_{cyt}$ and in the absence $\Delta A_{865}(0)$ of cytochrome. Control experiments are described in *SI Appendix*, section S3e.

Generation of Proton Gradient in RC@GUVs. Pyranine-containing RC@GUVs were prepared by including 10 μM pyranine in a modified I-solution (10 μM Tris·HCl, pH 7.0 and 200 mM sucrose). Potassium ferrocyanide (10 mM), cyt^{3+} (5 μM), and dQ (60 μM) were added to vesicles to allow the establishment of the photocycle (Fig. 3). Continuous light illumination was accomplished with a Schott KL 1500 illuminator equipped with a red-filtered 150-W lamp by using an optical light guide (1 inch in diameter) for irradiating the sample. Experiments were carried out by reading the increase of pyranine green fluorescence (*i*) as collective GUVs signal (by using a spectrofluorimeter) or (*ii*) as individual GUVs (by using a confocal microscope). Further details are given in *SI Appendix*, section S2i.

ACKNOWLEDGMENTS. This work was supported by Ministero dell'Istruzione, dell'Università e della Ricerca Grants 2010BJ23MN (Nanostructured Soft Matter) and PONa300369 (Laboratorio Sistema) and Apulia Region Project 31, "PHOEBUS" (Plastic Technologies for the Realization of Organic Solar Cells and High-Efficiency Bright and Uniform Sources). Collaboration among the authors has been fostered by the European COST Actions CM1304 (Emergence and Evolution of Complex Chemical Systems) and TD1102 (PHOTOTECH: Photosynthetic proteins for technological applications: biosensors and biochips).

1. Pohorille A, Deamer D (2002) Artificial cells: Prospects for biotechnology. *Trends Biotechnol* 20(3):123–128.
2. Noireaux V, Libchaber A (2004) A vesicle bioreactor as a step toward an artificial cell assembly. *Proc Natl Acad Sci USA* 101(51):17669–17674.
3. Kurihara K, et al. (2011) Self-reproduction of supramolecular giant vesicles combined with the amplification of encapsulated DNA. *Nat Chem* 3(10):775–781.
4. Kuruma Y, Stano P, Ueda T, Luisi PL (2009) A synthetic biology approach to the construction of membrane proteins in semi-synthetic minimal cells. *Biochim Biophys Acta* 1788(2):567–574.
5. Lentini R, et al. (2014) Integrating artificial with natural cells to translate chemical messages that direct E. coli behaviour. *Nat Commun* 5:4012.
6. Fujii S, et al. (2014) Liposome display for in vitro selection and evolution of membrane proteins. *Nat Protoc* 9(7):1578–1591.
7. Morowitz HJ, Heinz B, Deamer DW (1988) The chemical logic of a minimum protocell. *Orig Life Evol Biosph* 18(3):281–287.
8. Oberholzer T, Wick R, Luisi PL, Biebricher CK (1995) Enzymatic RNA replication in self-reproducing vesicles: an approach to a minimal cell. *Biochem Biophys Res Commun* 207(1):250–257.
9. Szostak JW, Bartel DP, Luisi PL (2001) Synthesizing life. *Nature* 409(6818):387–390.
10. Mansy SS, Szostak JW (2009) Reconstructing the emergence of cellular life through the synthesis of model protocells. *Cold Spring Harb Symp Quant Biol* 74:47–54.
11. de Lorenzo V, Danchin A (2008) Synthetic biology: Discovering new worlds and new words. *EMBO Rep* 9(9):822–827.
12. Luisi PL, Ferri F, Stano P (2006) Approaches to semi-synthetic minimal cells: A review. *Naturwissenschaften* 93(1):1–13.
13. Küchler A, Yoshimoto M, Luginbühl S, Mavelli F, Walde P (2016) Enzymatic reactions in confined environments. *Nat Nanotechnol* 11(5):409–420.
14. Kita H, et al. (2008) Replication of genetic information with self-encoded replicase in liposomes. *ChemBioChem* 9(15):2403–2410.
15. Gardner PM, Winzer K, Davis BG (2009) Sugar synthesis in a protocellular model leads to a cell signalling response in bacteria. *Nat Chem* 1(5):377–383.
16. Stano P, Carrara P, Kuruma Y, Souza TP, Luisi PL (2011) Compartmentalized reactions as a case of soft-matter biotechnology: Synthesis of proteins and nucleic acids inside lipid vesicles. *J Mater Chem* 21:18887–18902.
17. Nourian Z, Roelofsen W, Danelon C (2012) Triggered gene expression in fed-vesicle microreactors with a multifunctional membrane. *Angew Chem Int Ed Engl* 51(13):3114–3118.
18. Matsubayashi H, Kuruma Y, Ueda T (2014) In vitro synthesis of the E. coli Sec translocon from DNA. *Angew Chem Int Ed Engl* 53(29):7535–7538.
19. Grotzky A, et al. (2013) Structure and enzymatic properties of molecular dendronized polymer-enzyme conjugates and their entrapment inside giant vesicles. *Langmuir* 29(34):10831–10840.
20. Chen IA, Salehi-Ashtiani K, Szostak JW (2005) RNA catalysis in model protocell vesicles. *J Am Chem Soc* 127(38):13213–13219.
21. Mansy SS, et al. (2008) Template-directed synthesis of a genetic polymer in a model protocell. *Nature* 454(7200):122–125.
22. Kato A, Yanagisawa M, Sato YT, Fujiwara K, Yoshikawa K (2012) Cell-sized confinement in microspheres accelerates the reaction of gene expression. *Sci Rep* 2:283.
23. Dora Tang T-Y, van Swaay D, deMello A, Ross Anderson JL, Mann S (2015) In vitro gene expression within membrane-free coacervate protocells. *Chem Commun (Camb)* 51(57):11429–11432.
24. Bahatyrova S, et al. (2004) The native architecture of a photosynthetic membrane. *Nature* 430(7003):1058–1062.
25. Niederman RA (2016) Development and dynamics of the photosynthetic apparatus in purple phototrophic bacteria. *Biochim Biophys Acta* 1857(3):232–246.
26. Allen JP, Feher G, Yeates TO, Komiya H, Rees DC (1988) Structure of the reaction center from Rhodobacter sphaeroides R-26: Protein-cofactor (quinones and Fe2+) interactions. *Proc Natl Acad Sci USA* 85(22):8487–8491.
27. Stowell MH, et al. (1997) Light-induced structural changes in photosynthetic reaction center: Implications for mechanism of electron-proton transfer. *Science* 276(5313):812–816.
28. Junge W, Nelson N (2015) ATP synthase. *Annu Rev Biochem* 84:631–657.
29. Allen JP, Williams JC (1998) Photosynthetic reaction centers. *FEBS Lett* 438(1-2):5–9.
30. Pachence JM, Dutton PL, Blasie JK (1979) Structural studies on reconstituted reaction center-phosphatidylcholine membranes. *Biochim Biophys Acta* 548(2):348–373.
31. Overfield RE, Wraight CA (1980) Oxidation of cytochromes *c* and c_2 by bacterial photosynthetic reaction centers in phospholipid vesicles. 1. Studies with neutral membranes. *Biochemistry* 19(14):3322–3327.
32. Hellingwerf KJ (1987) Reaction centers from Rhodopseudomonas sphaeroides in reconstituted phospholipid vesicles. I. Structural studies. *J Bioenerg Biomembr* 19(3):203–223.
33. Venturoli G, Melandri BA, Gabellini N, Oesterhelt D (1990) Kinetics of photosynthetic electron transfer in artificial vesicles reconstituted with purified complexes from Rhodobacter capsulatus. I. The interaction of cytochrome c2 with the reaction center. *Eur J Biochem* 189(1):105–112.
34. Baciou L, Rivas E, Sebban P (1990) $P^+Q_A^-$ and $P^+Q_B^-$ charge recombinations in *Rhodopseudomonas viridis* chromatophores and in reaction centers reconstituted in phosphatidylcholine liposomes. Existence of two conformational states of the reaction centers and effects of pH and o-phenanthroline. *Biochemistry* 29(12):2966–2976.
35. Agostiano A, et al. (1995) Charge recombination of photosynthetic reaction centers in different membrane models. *Gazz Chim Ital* 125:615–622.
36. Hara M, et al. (1997) Orientation of photosynthetic reaction center reconstituted in neutral and charged liposomes. *Biosci Biotechnol Biochem* 61(9):1577–1579.
37. Palazzo G, Mallardi A, Giustini M, Berti D, Venturoli G (2000) Cumulant analysis of charge recombination kinetics in bacterial reaction centers reconstituted into lipid vesicles. *Biophys J* 79(3):1171–1179.
38. Trotta M, Milano F, Nagy L, Agostiano A (2002) Response of membrane protein to the environment: The case of photosynthetic reaction centre. *Mater Sci Eng C* 22:263–267.
39. Nagy L, et al. (2004) Protein/lipid interaction in the bacterial photosynthetic reaction center: Phosphatidylcholine and phosphatidylglycerol modify the free energy levels of the quinones. *Biochemistry* 43(40):12913–12923.
40. Milano F, et al. (2012) Light induced transmembrane proton gradient in artificial lipid vesicles reconstituted with photosynthetic reaction centers. *J Bioenerg Biomembr* 44(3):373–384.
41. Ollivon M, Lesieur S, Grabielle-Madelmont C, Paternostre M (2000) Vesicle reconstitution from lipid-detergent mixed micelles. *Biochim Biophys Acta* 1508(1-2):34–50.
42. Salafsky J, Groves JT, Boxer SG (1996) Architecture and function of membrane proteins in planar supported bilayers: A study with photosynthetic reaction centers. *Biochemistry* 35(47):14773–14781.
43. Schönfeld M, Montal M, Feher G (1979) Functional reconstitution of photosynthetic reaction centers in planar lipid bilayers. *Proc Natl Acad Sci USA* 76(12):6351–6355.
44. Packham NK, Packham C, Mueller P, Tiede DM, Dutton PL (1980) Reconstitution of photochemically active reaction centers in planar phospholipid membranes. Light-induced electrical currents under voltage-clamped conditions. *FEBS Lett* 110(1):101–106.
45. Gopher A, et al. (1985) The effect of an applied electric field on the charge recombination kinetics in reaction centers reconstituted in planar lipid bilayers. *Biophys J* 48(2):311–320.
46. Wang L, Roth JS, Han X, Evans SD (2015) Photosynthetic proteins in supported lipid bilayers: Towards a biokleptic approach for energy capture. *Small* 11(27):3306–3318.
47. Walde P, Cosentino K, Engel H, Stano P (2010) Giant vesicles: Preparations and applications. *ChemBioChem* 11(7):848–865.
48. Pautot S, Frisken BJ, Weitz DA (2003) Engineering asymmetric vesicles. *Proc Natl Acad Sci USA* 100(19):10718–10721.
49. Okamura MY, Steiner LA, Feher G (1974) Characterization of reaction centers from photosynthetic bacteria. I. Subunit structure of the protein mediating the primary photochemistry in Rhodopseudomonas spheroides R-26. *Biochemistry* 13(7):1394–1403.
50. Roth M, et al. (1989) Detergent structure in crystals of a bacterial photosynthetic reaction centre. *Nature* 340:659–662.
51. Sener MK, Olsen JD, Hunter CN, Schulten K (2007) Atomic-level structural and functional model of a bacterial photosynthetic membrane vesicle. *Proc Natl Acad Sci USA* 104(40):15723–15728.
52. Geyer T, Mol X, Blass S, Helms V (2010) Bridging the gap: Linking molecular simulations and systemic descriptions of cellular compartments. *PLoS One* 5(11):e14070.
53. Hassan Omar O, et al. (2016) Synthetic antenna functioning as light harvester in the whole visible region for enhanced hybrid photosynthetic reaction centers. *Bioconjug Chem* 27(7):1614–1623.
54. Milano F, et al. (2012) Enhancing the light harvesting capability of a photosynthetic reaction center by a tailored molecular fluorophore. *Angew Chem Int Ed Engl* 51(44):11019–11023.
55. Chiba M, Miyazaki M, Ishiwata S (2014) Quantitative analysis of the lamellarity of giant liposomes prepared by the inverted emulsion method. *Biophys J* 107(2):346–354.
56. Gopta OA, Semenov AY, Bloch DA (2001) Electrogenic proton transfer in *Rhodobacter sphaeroides* reaction centers: Effect of coenzyme Q(10) substitution by decylubiquinone in the Q(B) binding site. *FEBS Lett* 499(1-2):116–120.
57. Yanagisawa M, Iwamoto M, Kato A, Yoshikawa K, Oiki S (2011) Oriented reconstitution of a membrane protein in a giant unilamellar vesicle: Experimental verification with the potassium channel KcsA. *J Am Chem Soc* 133(30):11774–11779.
58. Luo TJM, Soong R, Lan E, Dunn B, Montemagno C (2005) Photo-induced proton gradients and ATP biosynthesis produced by vesicles encapsulated in a silica matrix. *Nat Mater* 4(3):220–224.
59. Dezi M, Di Cicco A, Bassereau P, Lévy D (2013) Detergent-mediated incorporation of transmembrane proteins in giant unilamellar vesicles with controlled physiological contents. *Proc Natl Acad Sci USA* 110(18):7276–7281.
60. Feng X, Jia Y, Cai P, Fei J, Li J (2016) Coassembly of photosystem II and ATPase as artificial chloroplast for light-driven ATP synthesis. *ACS Nano* 10(1):556–561.
61. Steinberg-Yfrach G, et al. (1997) Conversion of light energy to proton potential in liposomes by artificial photosynthetic reaction centres. *Nature* 385:239–241.